Supplementary Information for
Tunable multi-bands in twisted double bilayer graphene

Yujian Zhu[1†], Yiwei Chen[1†], Qingxin Li[1†], Yongdao Chen[2], Yan Huang[1], Wang Zhu[1], Dongdong An[1], Junwei Song[1], Qikang Gan[1], Kaiyuan Wang[1], Lingnan Wei[1], Qijun Zong[1], Kenji Watanabe[3], Takashi Taniguchi[3], Haolin Wang[1], Li Huang[2], Lede Xian[4,5], Liang Sun[1], Geliang Yu[1*], and Lei Wang[1*]

[1]*National Laboratory of Solid-State Microstructures, School of Physics, Nanjing University, Nanjing, 210093, China*

[2]*Department of Physics, Southern University of Science and Technology, Shenzhen 518055, China*

[3]*National Institute for Materials Science, Namiki 1-1, Tsukuba, Ibaraki 305-0044, Japan*

[4]*Songshan Lake Materials Laboratory, Dongguan, Guangdong,523808, China*

[5]*Center for free Electron Laser Science, Max Planck Institute for the Structure and Dynamics of Matter, Hamburg, 22761, Germany*

[6]*School of Advanced Materials and Nanotechnology Xidian University Xi'an, Shaanxi,710071, P. R. China*

[†]*These authors contributed equally to this work. and*

[*]*Corresponding authors, Email: yugeliang@nju.edu.cn; leiwang@nju.edu.cn*

SAMPLE FABRICATION AND MEASUREMENT SETUP

The device in our text was encapsulated between flakes of hexagonal boron nitride(hBN) with thickness about 30nm. The raw materials for the preparation of devices, hexagonal boron nitride(hBN) and bilayer graphene are obtained from mechanically exfoliation onto Si/SiO_2 substrate. Their thickness and quality were then identified by optical microscopy and atomic force microscopy. Stack of BN/tDBG/BN was assembled using dry pick-up technique with a stamp consisting of polyproylene carbonate(PPC) film and polydimethylsiloxane(PDMS). The stack is then annealed under high vacuum at $350°C$. Next we defined the geometry of the topgate and channel using electron beam lithography and reactive ion etching. Afterwards the electrode contact and topgate were evaporated by Cr/Pd/Au(5nm/15nm/100nm) and Ti/Au(5nm/30nm) respectively by e-beam evaporation. Transport measurement were carried out in cryogenic superconducting magnets with base temperature of 1.5K. The four-terminal resistance were measured using low-frequency lock-in techniques at 17.777Hz with a current excitation of $100nA$ or a voltage excitation of $100\mu V$.

TWIST ANGLE DETERMINATION

We first estimate the angle by the value of the carrier density corresponding to the full filling gap. For small angles, the following formula can be calculated:

$$n_s = 4/A \approx \frac{\sqrt{3}a^2}{8\theta^2}$$

where $a = 0.246nm$ is the lattice constant of graphene, A is the area of moiré unit cell and n_s is the carrier density at the 1st full filling of moiré band. Precise determination of the angle is obtained by exploiting the Hofstadter spectral signature in the magnetic field. The intersection of Landau fan is at the point where the magnetic flux in a moiré unit cell is a fraction of the flux quantum($\phi = BA = \phi_0/q$, where q is a integer). After determining the value of A, we can also confirm the angle.

BAND STRUCTURE CALCULATIONS

We calculate the electronic structure of twisted double bilayer graphene using the full-lattice tight-binding method. The tight-binding Hamiltonian of twisted double bilayer graphene is written in the following form:

$$H = \sum_i \varepsilon_i |i\rangle\langle i| + \sum_{i,j} t_{ij} |i\rangle\langle j|$$

$$t_{ij} = n_{ij}^2 V_\sigma(r_{ij}) + (1 - n_{ij}^2 V_\pi(r_{ij}))$$

$$|i\rangle\langle j| = e^{i\vec{K}(\vec{r}_j - \vec{r}_i)}$$

$$n_{ij} = \frac{z_{ij}}{r_{ij}}$$

where t_{ij} is the coupling matrix element calculated as in ref[1, 2], r_{ij} is the distance between atomic sites i and j, andZ_{ij} is the projection of r_{ij} along the out-of-plane direction (z-axis). We use the following Slater and Koster parameters:

$$V_\sigma(r_{ij}) = \gamma_1 e^{\frac{q_\sigma}{a}(a - r_{ij})} F_c(r_{ij})$$

$$V_\pi(r_{ij} = -\gamma_0 e^{\frac{q_\pi}{d}(d - r_{ij})} F_c(r_{ij}))$$

where a is the nearest distance between carbon atoms in the same layer($1.42\mathring{A}$), d is the interlayer distance, $\gamma_0 = 3.24eV$ is the nearest-neighbor hopping parameter, $\gamma_1 = 0.48eV$ is the magnitude of the interlayer hopping in the AB/BA regions, $\frac{q_\sigma}{a}$and$\frac{q_\pi}{d}$ are set to be $2.218\mathring{A}^{-1}$, which fixes the value of second-neighbors interaction. F_c is a smooth cutoff function defined as:

$$F_c(r) = (1 + e^{(r - r_c)/l_c})^{-1}$$

where $r_c = 6.14\mathring{A}$ is the cutoff distance, and $l_c = 0.265\mathring{A}$. The effects of electric field are considered by adding an on-site energy term $\epsilon_i = E \cdot z_i$ to the Hamiltonian, where E is the strength of the electric field and z_i is the atomic coordinate along z-axis. It has been shown that the structural relaxation of twisted graphene affects the band structure[3, 4]. Here, we fully relax the carbon atoms using the molecular dynamics code LAMMPS[5].

THE EFFECT OF CRYSTAL FIELD

In twisted multilayer graphene, because of the different environment between the inner and the outer layers, internal crystal field could exist and affect the electronic structure of the system[4, 6, 7]. In order to evaluate such effect, we perform further calculations that include crystal field following the method outlined in Ref. 4 and compare the results with the experiments. With zero displacement field, the calculation without displacement field gives a band gap of 3.62 meV at the CNP, stemming purely from the interlayer hopping [8, 9]. After including the effect of the crystal field, the band gap at the CNP is closed (Fig. S10(b)). This result is consistent with the previous work [4] and it indeed gives a better agreement with the experiments. The gap closure at the CNP results from the competition between the intrinsic band gap and the gap induced by displacement field. We further check the crystal field effects with finite displacement field.

With applied displacement field, as shown in Fig. S10(c) and (d), the results calculated with and without crystal field share some similar features. In particular, the gaps at the full-filling at both the electron and the hole sides can be closed and re-opened by displacement field. This feature is in qualitative agreement with the experiments and confirm that the gaps observed in experiments are trivial band gaps and not correlated gaps. However, the overall gap sizes at different fillings calculated without crystal field show better agreement with the experimental results (see Fig.2 in the main text). This could due to the change of the Hartree potentials and the reduction of the crystal field due to the dielectric environment of the substrate as shown in a recent calculation[10]. Therefore, we still present the TB results without crystal field as a good approximation to show the tunable multi-band features in TDBG.

FITTING PROCEDURES

A fitting of the resistance versus inverse of temperature exponential relationship is done in obtaining the thermal activation gap($R \propto exp(\Delta/2k_bT)$). The other fitting is a T-linear and T-square fit for each carrier density in the phase diagram of resistance versus temperature and carrier density, and make a judgment on which one belongs according to the comparison of the goodness of fit. Theses were all done using the MATLAB Fitting Toolkit.

S1: OPTICAL IMAGE OF DEVICE

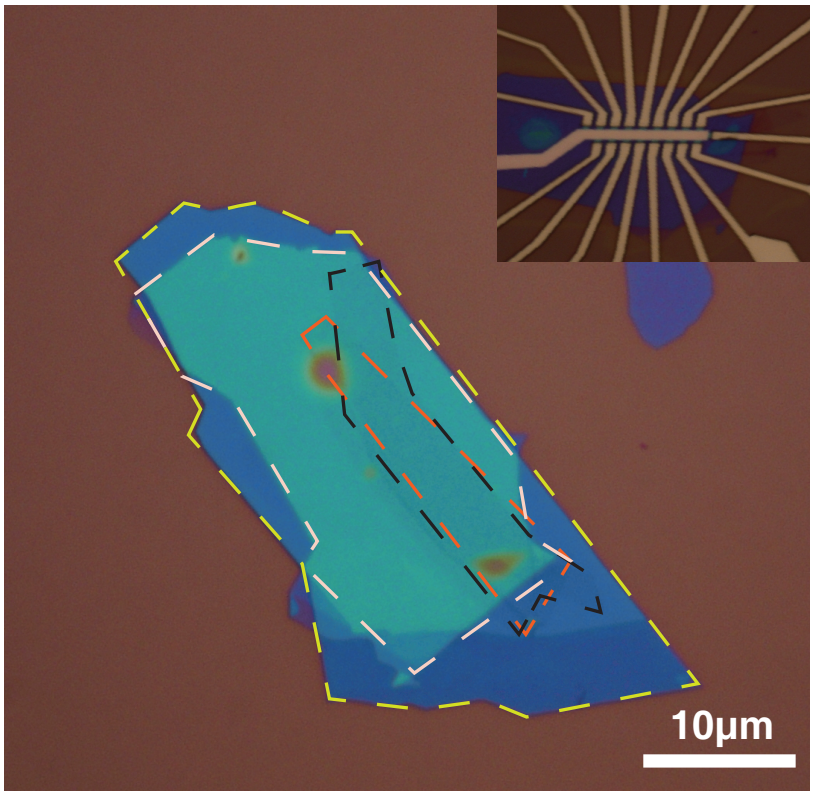

SUPPLEMENTARY FIG. 1: Optical image of 1.05° stack in the text. The dashed lines mark each layer, where red and black denote two bilayer graphene sheets, yellow and flesh denote hexagonal boron nitride. The top right figure shows the optical view of the device.

S2: CALCULATED DOS OF 1.05°TDBG

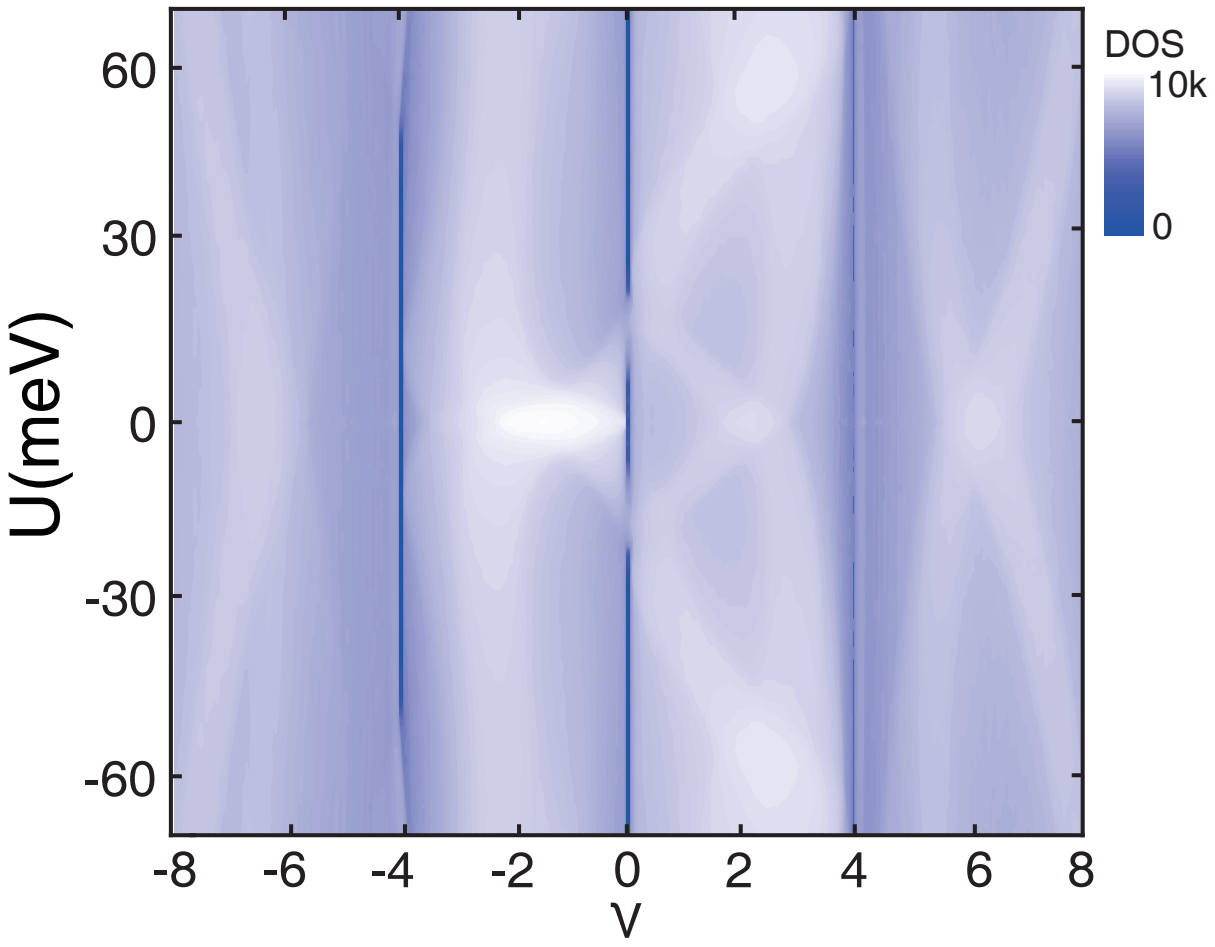

SUPPLEMENTARY FIG. 2

S3: ARRHENIUS FITS FOR 1ST FULL FILLING

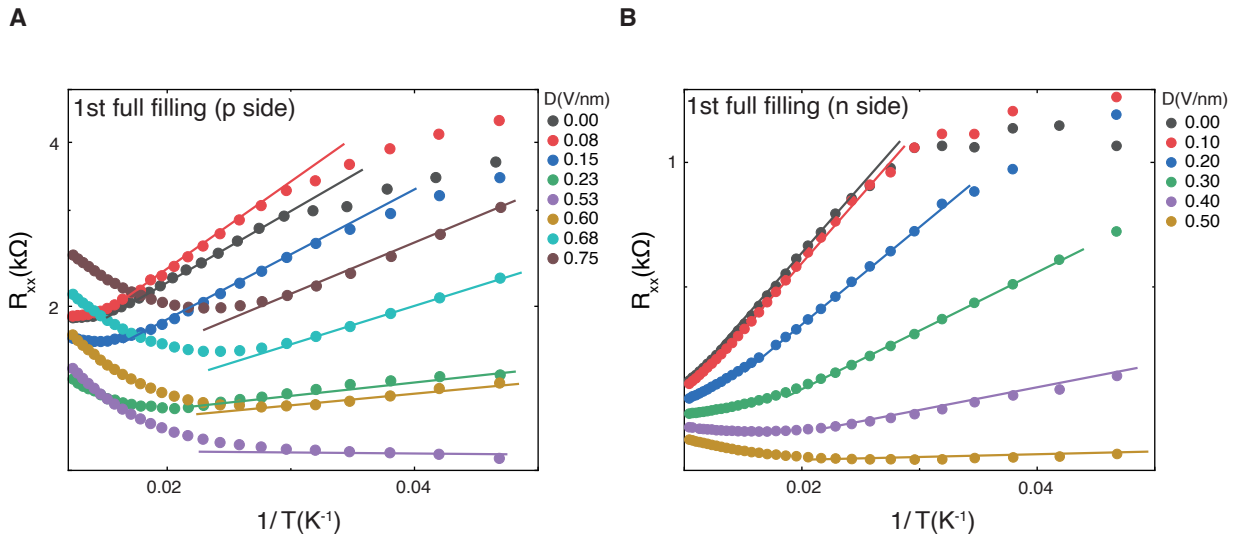

SUPPLEMENTARY FIG. 3: Arrhenius fit for 1st full filling. **A,** Fit for p side.**B,** Fit for n side.

S4: ARRHENIUS FITS FOR 3RD FULL FILLING

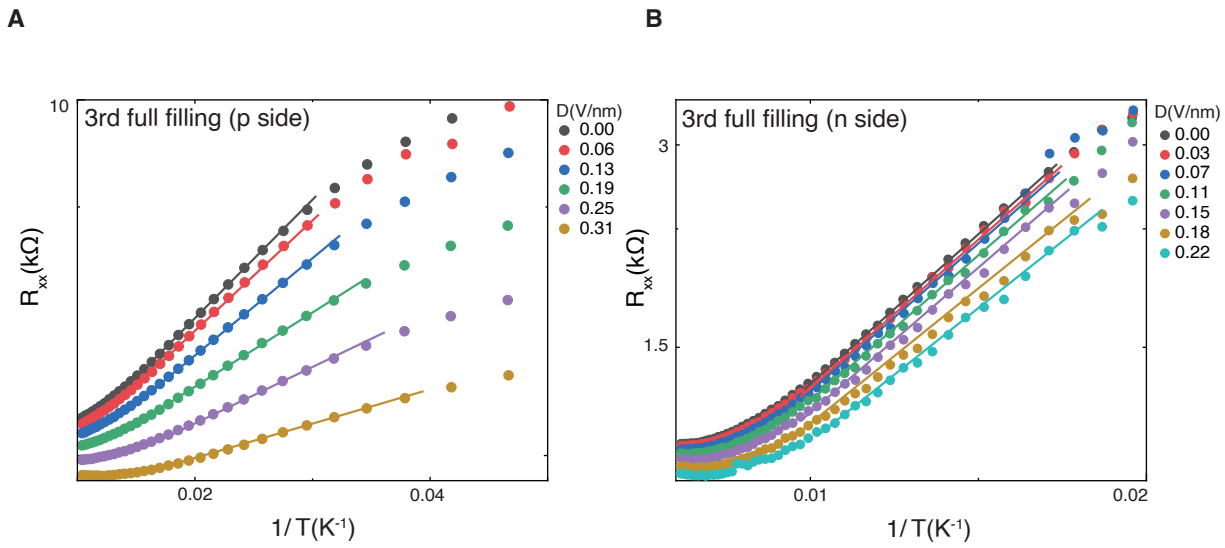

SUPPLEMENTARY FIG. 4: Arrhenius fit for 3rd full filling. **A,** Fit for p side.**B,** Fit for n side.

S5: ARRHENIUS FITS FOR CHARGE NEUTRAL POINT

.

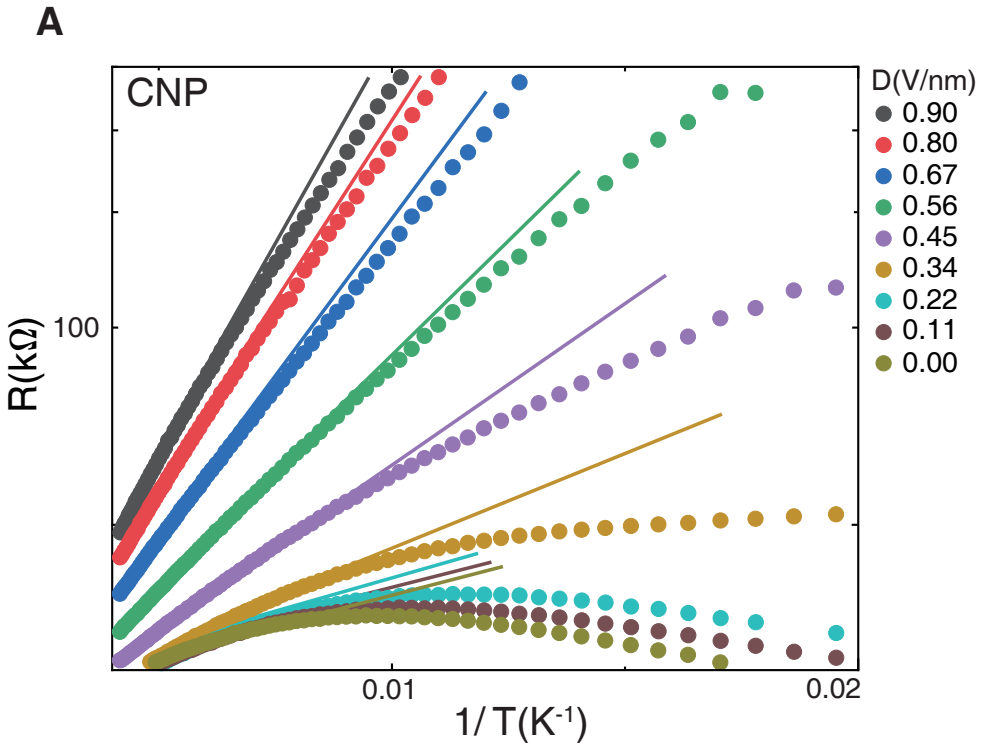

SUPPLEMENTARY FIG. 5: Arrhenius fit for charge neutral point(CNP).

S6:ANOMALOUS BEHAVIOR OF THE CNP

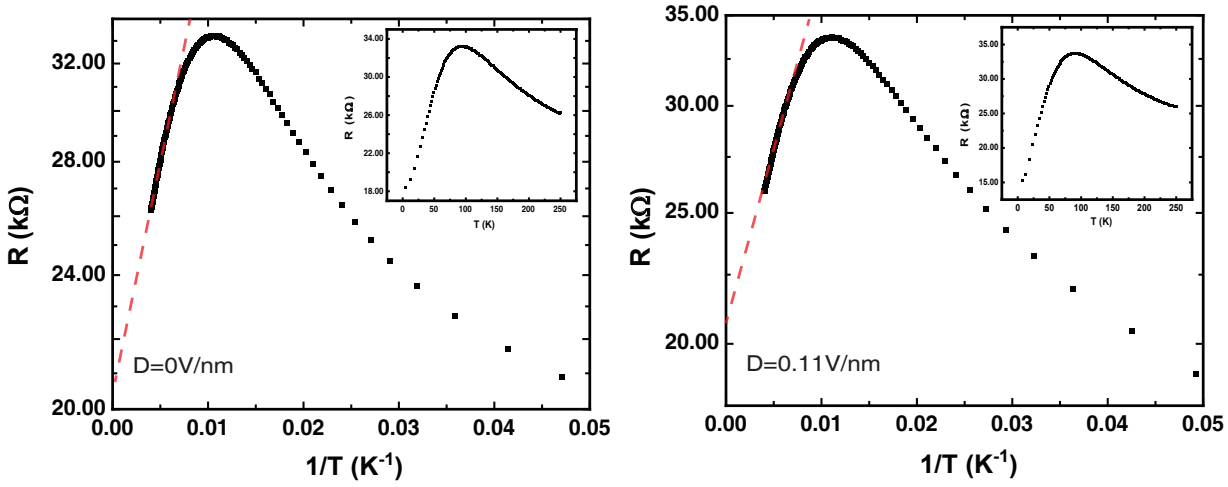

SUPPLEMENTARY FIG. 6: Arrhenius fit for $D = 0V/nm$ and $D = 0.11V/nm$ at CNP, the inset diagrams show the resistance versus temperature.

S7:PHASE DIAGRAM OF FULL FILLING GAPS

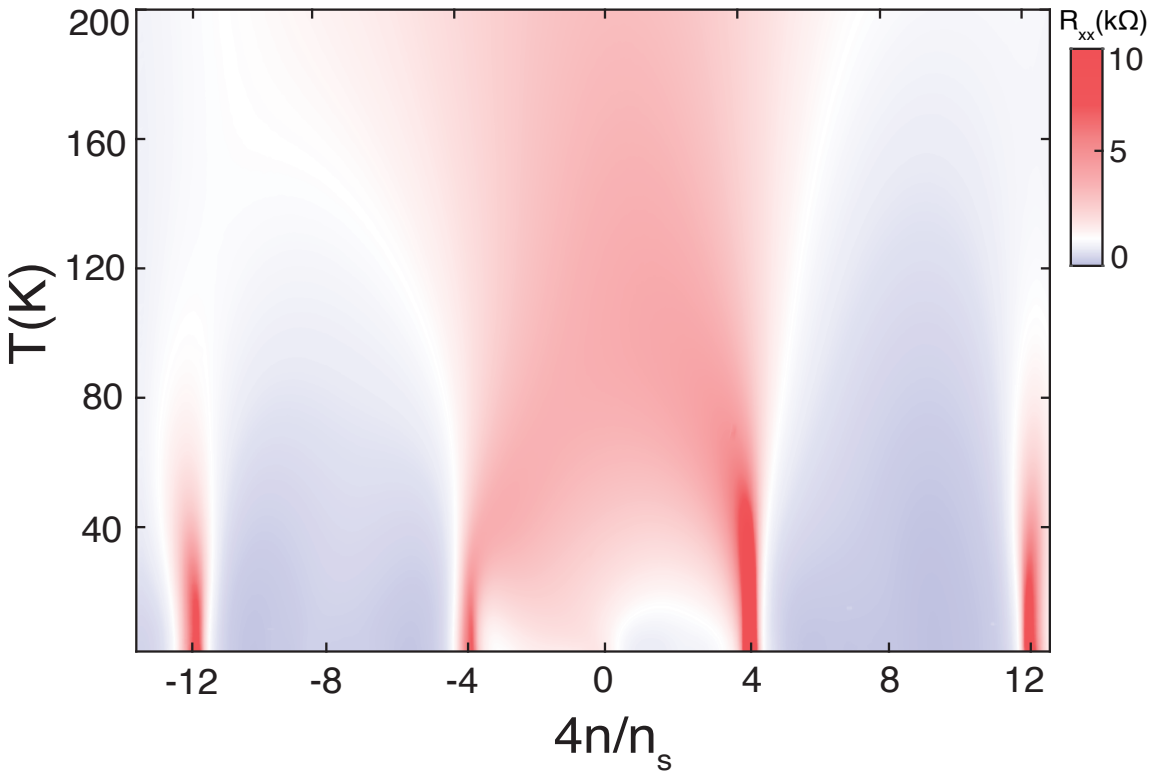

SUPPLEMENTARY FIG. 7: Phase diagram of full filling gaps. Plot of longitudinal resistance versus temperature and normalized carrier density at $D = 0V/nm$

S8: DECOUPLING FRATURE AT DIFFERENT MAGNETIC FIELDS

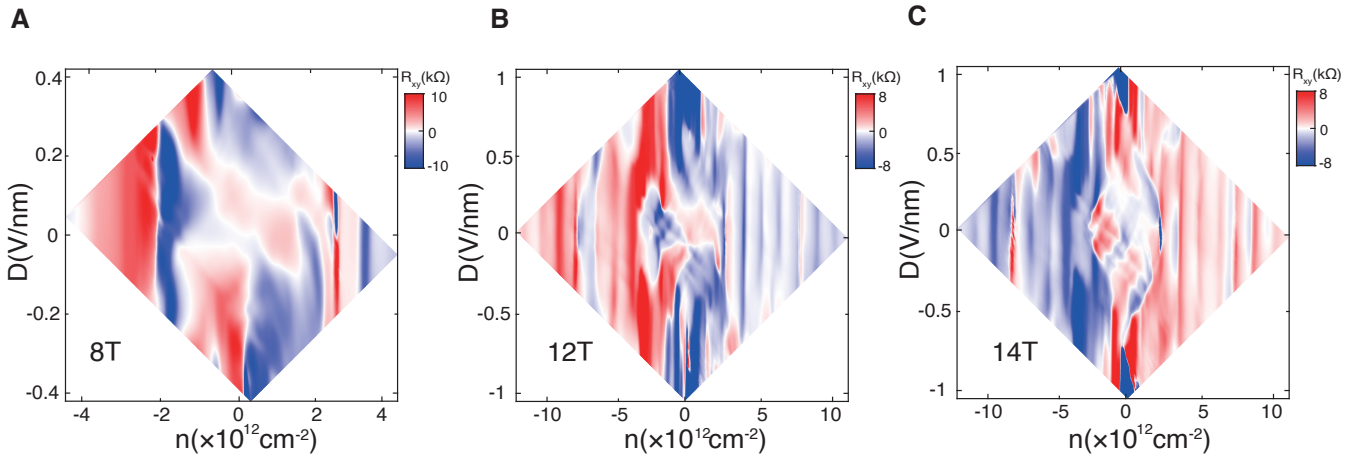

SUPPLEMENTARY FIG. 8: Mapping of the Hall resistance as a function of carrier density n and displacement field D. **A,** $B = 8T$. **B,** $B = 12T$. **C,** $B = 14T$.

S9: OTHER DEVICES WITH SIMILAR TWISTED ANGLE

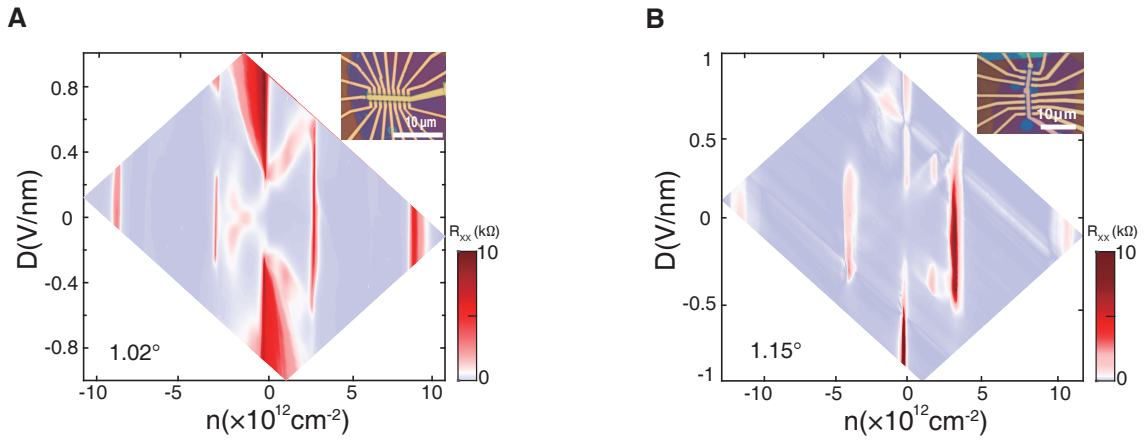

SUPPLEMENTARY FIG. 9: Two devices with similar twisted angle reveal similar band structure.

S10: BAND STRUCTURE CALCULATION WITH AND WITHOUT CRYSTAL FIELD

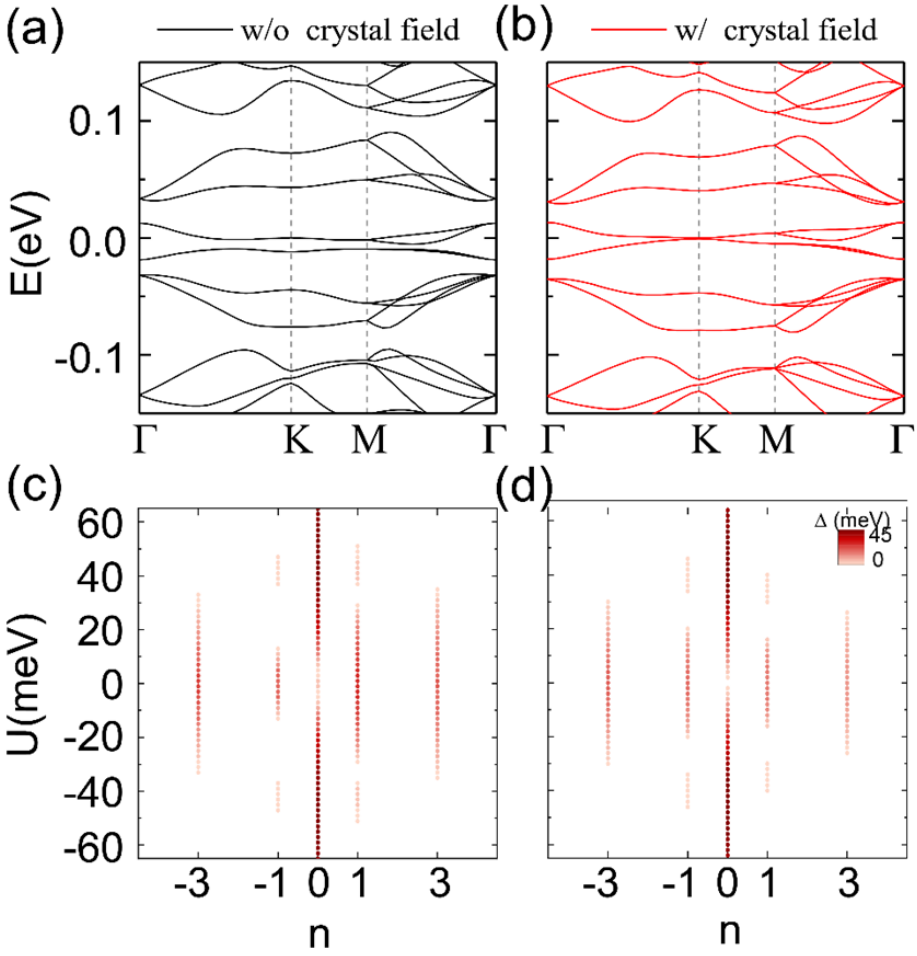

SUPPLEMENTARY FIG. 10: (a-b) Band structures of TDBG calculated with (a) and without (b) crystal field at zero displacement field. (c-d) Calculated gap sizes at different fillings with displacement field U with (c) and without (d) crystal field.

[1] P. Moon and M. Koshino, Phys. Rev. B **87**, 205 (2013).

[2] J. C. Slater and G. F. Koster, Phys. Rev. **94**, 1498 (1954).

[3] N. N. T. Nam and M. Koshino, Physical Review B **96**, 075311 (2017).

[4] F. Haddadi, Q. Wu, A. J. Kruchkov, and O. V. Yazyev, Nano Letters **20**, 2410 (2020).

[5] S. Plimpton, Journal of Computational Physics **117**, 1 (1995).

[6] P. Rickhaus, G. Zheng, J. L. Lado, Y. Lee, A. Kurzmann, M. Eich, R. Pisoni, C. Tong, R. Garreis, C. Gold, M. Masseroni, T. Taniguchi, K. Wantanabe, T. Ihn, and K. Ensslin, Nano Letters **19**, 8821 (2019).

[7] F. J. Culchac, R. R. Del Grande, R. B. Capaz, L. Chico, and E. S. Morell, Nanoscale **12**, 5014 (2020).

[8] N. R. Chebrolu, B. L. Chittari, and J. Jung, Phys. Rev. B **99**, 235417 (2019).

[9] Y. W. Choi and H. J. Choi, Phys. Rev. B **100**, 201402 (2019).

[10] C. T. S. Cheung, Z. A. H. Goodwin, V. Vitale, J. Lischner, and A. A. Mostofi, Electronic Structure **4**, 025001 (2022).